MULTIGRID PRECONDITIONING FOR TIME-HARMONIC MAXWELL'S EQUATIONS IN 3D

D.A. ARULIAH* AND U.M. ASCHER†

Abstract. We consider the rapid simulation of three-dimensional electromagnetic problems in parameter regimes where the quasi-static approximation applies, the permeability is constant, the conductivity may vary significantly, and the range of frequencies is moderate. The difficulties encountered include handling solution discontinuities across interfaces and accelerating convergence of traditional iterative methods for the solution of the linear systems of algebraic equations that arise when discretizing Maxwell's equations in the frequency domain.

In previous works, we used a potential-current formulation combined with a pressure-Poisson-like differentiation in order to pose the differential system in a weakly-coupled elliptic form. A finite-volume discretization on a staggered grid was subsequently employed to arrive at a large, sparse, linear system of equations with a block-diagonally dominant structure. A preconditioned BiCGStab iteration, where the diagonal blocks were approximately inverted by an ILU-decomposition, was found to be particularly efficient for solving the latter system.

In this paper, we first provide a Fourier analysis to show that inverting the diagonal blocks of the reformulated system indeed yields an efficient preconditioner. We then consider replacing the full inversion of these diagonal blocks by just one multigrid cycle, and extend the Fourier analysis to show that the condition number of the resulting preconditioned matrix is still bounded independent of the grid.

Finally, we present numerical examples for more realistic situations involving large variations in conductivity (i.e. jump discontinuities). Block-preconditioning with one multigrid cycle using J. Dendy's BOXMG solver is found to yield convergence in very few iterations, apparently independent of the grid size. The experiments show that the somewhat restrictive assumptions of the Fourier analysis do not prohibit it from describing the essential local behaviour of the preconditioned operator under consideration. A very efficient, practical solver is obtained.

Keywords: Multigrid preconditioning, Maxwell's equations, finite volume, Krylov methods, Coulomb gauge, solution discontinuities.

1. Introduction.

The need for calculating fast, accurate solutions of three-dimensional electromagnetic equations arises in many important application areas including, among others, geophysical surveys and medical imaging [5, 6, 19, 22, 28]. In remote sensing inverse problems, e.g. in geophysics, dozens, if not hundreds, of such systems are solved in the course of one data inversion. Consequently, there is much current interest in finding efficient numerical algorithms [4, 14, 18, 23].

Assuming a time-dependence $e^{-\imath\omega t}$, Maxwell's equations in a three-dimensional domain Ω read

$$\nabla\times\ \boldsymbol{E} - \imath\omega\mu\boldsymbol{H} = \boldsymbol{0}, \tag{1.1a}$$
$$\nabla\times\ \boldsymbol{H} - \widehat{\sigma}\boldsymbol{E} = \boldsymbol{J^s}, \tag{1.1b}$$

where μ is the magnetic permeability and $\boldsymbol{J^s}$ is a known electric source current density. Also,

$$\widehat{\sigma} = \sigma - \imath\omega\epsilon, \tag{1.2}$$

where σ is the conductivity and ϵ the electrical permittivity. The electric field $\boldsymbol{E}$ and the magnetic field $\boldsymbol{H}$ are unknown, as is the charge density ρ defined by

$$\nabla\cdot(\epsilon\boldsymbol{E}) = \rho. \tag{1.3}$$

*Department of Computer Science, University of British Columbia, Vancouver, BC, V6T 1Z4, Canada. (dhavide@cs.ubc.ca). Supported in part under NSERC CRD Grant 80357.

†Department of Computer Science, University of British Columbia, Vancouver, BC, V6T 1Z4, Canada. (ascher@cs.ubc.ca). Supported in part under NSERC Research Grant 84306.

The known physical properties $\epsilon > 0$, $\mu > 0$, and $\sigma \geq 0$ can vary with position and are assumed bounded and piecewise smooth. The frequency range under consideration is restricted so that $\mu\epsilon\omega^2 L^2 \ll 1$, where L is a typical length scale [29]. Typical boundary conditions for (1.1) are described in [15, 16].

In [2, 15, 16], we solve this problem numerically as follows:

1. The PDE system is first transformed into a weakly-coupled elliptic form. This is achieved by applying a Helmholtz decomposition

$$\boldsymbol{E} = \boldsymbol{A} + \nabla\phi, \tag{1.4a}$$
$$\nabla \cdot \boldsymbol{A} = 0, \tag{1.4b}$$

as in [12], then adding a stabilization term and replacing (1.4b) by the simplified divergence of (1.1b). The resulting equations are

$$\begin{aligned} &-\nabla\times\left(\mu^{-1}\nabla\times\boldsymbol{A}\right) + \nabla\left(\mu^{-1}\nabla\cdot\boldsymbol{A}\right) + \imath\omega\widehat{\sigma}\left(\boldsymbol{A}+\nabla\phi\right) \\ &\qquad = -\imath\omega\boldsymbol{J^s}, \end{aligned} \tag{1.5a}$$
$$\nabla\cdot\left(\widehat{\sigma}\left(\boldsymbol{A}+\nabla\phi\right)\right) = -\nabla\cdot\boldsymbol{J^s}. \tag{1.5b}$$

A further assumption often made (e.g. [21, 27]) is to keep $\mu \equiv \mu_0$ constant. Then, (1.5) simplifies into

$$\nabla^2\boldsymbol{A} + \imath\omega\mu\widehat{\sigma}\left(\boldsymbol{A}+\nabla\phi\right) = -\imath\omega\mu\boldsymbol{J^s}, \tag{1.6a}$$
$$\nabla\cdot\left(\widehat{\sigma}\left(\boldsymbol{A}+\nabla\phi\right)\right) = -\nabla\cdot\boldsymbol{J^s}. \tag{1.6b}$$

Appropriate boundary conditions for (1.5), corresponding, for instance, to

$$\boldsymbol{H}\times\boldsymbol{n}\Big|_{\partial\Omega} = 0,$$

are

$$\left(\nabla\times\boldsymbol{A}\right)\times\boldsymbol{n}\Big|_{\partial\Omega} = \boldsymbol{0} \tag{1.7a}$$
$$\boldsymbol{A}\cdot\boldsymbol{n}\Big|_{\partial\Omega} = 0 \tag{1.7b}$$
$$\widehat{\sigma}(\boldsymbol{A}+\nabla\phi)\cdot\boldsymbol{n}\Big|_{\partial\Omega} = -\boldsymbol{J^s}\cdot\boldsymbol{n}\Big|_{\partial\Omega} \tag{1.7c}$$
$$\int_\Omega \phi\, dV = \int_\Omega \left(\mu^{-1}\nabla\cdot\boldsymbol{A}\right)\, dV = 0. \tag{1.7d}$$

2. The transformed PDE system is discretized next. To handle large jumps in conductivity σ, a staggered discretization scheme is used [15, 16]. The resulting large, sparse linear system of equations has a block-diagonally dominant form. In the case (1.6), which we will assume in this work, the diagonal blocks are in fact discretizations of the differential operators $\nabla^2 + \imath\omega\mu_0\widehat{\sigma}$ (three blocks) and $\nabla\cdot(\widehat{\sigma}\nabla(\cdot))$ equipped with suitable boundary conditions. The off-diagonal blocks involve discretizations of $\imath\omega\mu\widehat{\sigma}\nabla(\cdot)$ and $\nabla\cdot\widehat{\sigma}$. For completeness, we provide a few additional details on the discretization in Section 2.
3. A BiCGStab Krylov method (e.g., [3, 25]) is found to perform efficiently in conjunction with preconditioning by Incomplete LU-decomposition (ILU)

with a permissive threshold applied to the real part of the diagonal blocks. Note that the real part of $\hat{\sigma}$ is slightly regularized, viz., in the preconditioner

$$\sigma \leftarrow \max(\sigma, \sigma_a), \tag{1.8}$$

with $\sigma_a > 0$ small (on the order of 10^{-9} to 10^{-6}).

One purpose of the current work is to supply some theoretical basis for the latter observation on the block-diagonal preconditioner for the Krylov iteration. Thus, in Section 3, we apply a Fourier analysis [7, 8, 11, 17, 24] to show that if the real part of the diagonal blocks of the discretization of (1.6) is used as a preconditioner (i.e. these 4 Poisson problems are inverted exactly), then indeed the ranges of the eigenvalues and of the singular values are bounded independently of the grid size. These range sizes grow quadratically as a function of the parameter

$$\chi := \omega\mu\sigma \tag{1.9}$$

(which corresponds to the term ignored by the preconditioner under the notation-simplifying assumption that $\widehat{\sigma} = \sigma$).

The Fourier analysis requires the assumptions that all coefficients are constant (in particular $\widehat{\sigma}$), that the problem is discretized on a uniform grid, and that the grid is infinite in extent or that the boundary conditions are periodic. The first of these assumptions is especially unrealistic; however, the theoretical results of Section 3 are corroborated by numerical examples in Section 4, where we allow $\widehat{\sigma} \neq \sigma$ to have very large jump discontinuities.

We further extend our theoretical results for the case where the preconditioner consists of just one multigrid W-cycle for the real part of the diagonal blocks (Section 3). The possibility that just one multigrid cycle would be sufficiently powerful as a preconditioner to yield grid-independent convergence rates was noted earlier in other contexts by various researchers (see, e.g., [20] and references therein). For the implementation of the multigrid preconditioner, we use Dendy's BOXMG code [9, 10]. In the general case of variable coefficients with jumps, this yields a very efficient practical solver, as demonstrated in Section 4.

2. Finite volume discretization. Assume that Ω^h is the unit cube $[0,1]^3$ divided into a uniform $n \times n \times n$ union of non-overlapping cells of width $h := 1/n$ (this is a simplification of the grids considered in [2, 16]). The material properties $\widehat{\sigma}$ are assumed constant through each cell. Further, assume that the current source $\boldsymbol{J^s}$ has no layers and that the normal components of $\boldsymbol{J^s}$ across cell interfaces are continuous.[1] Let $(A^x, A^y, A^z)^T$ denote the components of the vector potential field $\boldsymbol{A}$ in Cartesian coordinates. The corresponding discrete fields $\boldsymbol{A}^h$ and ϕ^h are defined on a staggered grid, as illustrated in Figure 2.1. In particular, the discrete values ${A^x}_{i+\frac{1}{2},j,k}$, ${A^y}_{i,j+\frac{1}{2},k}$ and ${A^z}_{i,j,k+\frac{1}{2}}$ lie in the centers of corresponding cell faces and the discrete values $\phi_{i,j,k}$ lie at the centers of cells.

As in [2, 16], the coefficient matrix for the discretized equations is

$$A := \begin{pmatrix} \boldsymbol{\Delta}^h + \imath\omega\mu\widehat{\sigma}^h & \imath\omega\mu\widehat{\sigma}^h(\nabla)^h \\ (\nabla\cdot)^h\widehat{\sigma}^h & (\nabla\cdot)^h\widehat{\sigma}^h(\nabla)^h \end{pmatrix} \tag{2.1}$$

Here, the blocks are discretizations of various operators on a staggered grid subject to suitable boundary conditions. The matrix $(\nabla)^h$ is the discretization of the gradient

[1] In practice, the grid is chosen such that source singularities, if they occur, are contained inside grid cells

FIG. 2.1. *Staggered grid discretization. The discrete vector field $\boldsymbol{A}^h$ at centers of cell faces & the discrete scalar field ϕ^h at centers of cells.*

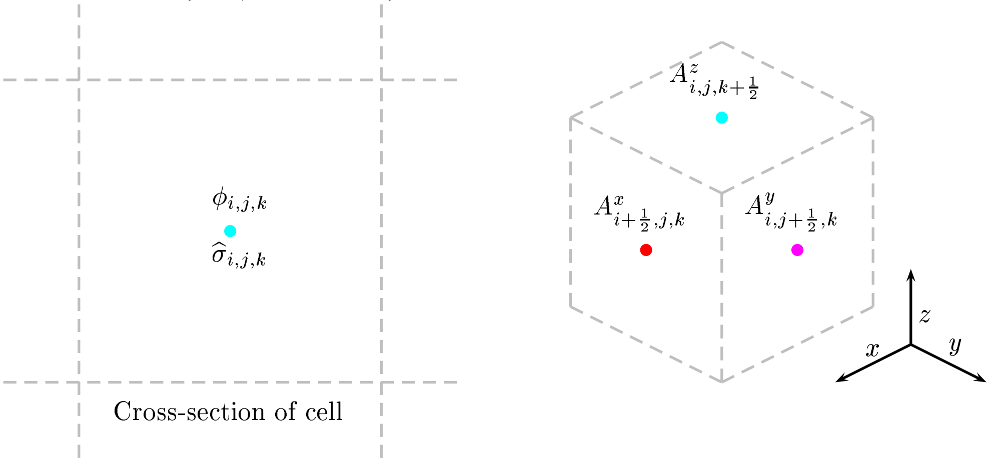

operator; $(\nabla\cdot)^h$ is the discretization of the divergence operator; $\widehat{\sigma}^h$ is the staggered grid discretization of the operator $\widehat{\sigma}I$ (using harmonic averages of values of $\widehat{\sigma}$ in adjacent cells, e.g., [26]); and $\boldsymbol{\Delta}^h$ is the discretization of the *vector* Laplacian operator. Notice that $\boldsymbol{\Delta}^h$ and $\widehat{\sigma}^h$ are in turn 3×3 block matrices that act on the space of discrete vector fields with components normal to cell faces. Further, $(\nabla)^h$ is a 3×1 block matrix (mapping discrete scalar fields to discrete vector fields) and $(\nabla\cdot)^h$ is a 1×3 block matrix (mapping discrete vector fields to discrete scalar fields).

Considering (2.1) as a 4×4 block matrix, the operators in the first block row of A are

$$\begin{aligned}
\left[\Delta^h A^{x\,h}\right]_{i+\frac{1}{2},j,k} + \imath\omega\mu\widehat{\sigma}_{i+\frac{1}{2},j,k} &= \frac{1}{h^2}\Big({A^x}_{i+\frac{3}{2},j,k} + {A^x}_{i+\frac{1}{2},j+1,k} + {A^x}_{i+\frac{1}{2},j,k+1} \\
&\quad + {A^x}_{i-\frac{1}{2},j,k} + {A^x}_{i+\frac{1}{2},j-1,k} + {A^x}_{i+\frac{1}{2},j,k-1} \\
&\quad + (-6 + h^2\imath\omega\mu\widehat{\sigma}_{i+\frac{1}{2},j,k}){A^x}_{i+\frac{1}{2},j,k}\Big)\,, \qquad (2.2a)\\
\left[(\widehat{\sigma}^h(\nabla)^h)^x\phi^h\right]_{i+\frac{1}{2},j,k} &= \frac{1}{h}\widehat{\sigma}_{i+\frac{1}{2},j,k}\left(\phi_{i+1,j,k} - \phi_{i,j,k}\right). \qquad (2.2b)
\end{aligned}$$

See [16] for details. The second and third block rows are defined analogously. The last block row is centered at cell centers and defined by

$$
\begin{aligned}
\left[(\nabla\cdot)^h\widehat{\sigma}^h\boldsymbol{A}^h\right]_{i,j,k} = \frac{1}{h}\Big(&\widehat{\sigma}_{i+\frac12,j,k}{A^x}_{i+\frac12,j,k} - \widehat{\sigma}_{i-\frac12,j,k}{A^x}_{i-\frac12,j,k} \\
&+ \widehat{\sigma}_{i,j+\frac12,k}{A^y}_{i,j+\frac12,k} - \widehat{\sigma}_{i,j-\frac12,k}{A^y}_{i,j-\frac12,k} \\
&+ \widehat{\sigma}_{i,j,k+\frac12}{A^z}_{i,j,k+\frac12} - \widehat{\sigma}_{i,j,k-\frac12}{A^z}_{i,j,k-\frac12}\Big), \qquad (2.3a)
\end{aligned}
$$

$$
\begin{aligned}
\left[(\nabla\cdot)^h\widehat{\sigma}^h(\nabla)^h\phi^h\right]_{i,j,k} = \frac{1}{h^2}\Big(&\widehat{\sigma}_{i+\frac12,j,k}\phi_{i+1,j,k} + \widehat{\sigma}_{i,j+\frac12,k}\phi_{i,j+1,k} + \widehat{\sigma}_{i,j,k+\frac12}\phi_{i,j,k+1} \\
&+ \widehat{\sigma}_{i-\frac12,j,k}\phi_{i-1,j,k} + \widehat{\sigma}_{i,j-\frac12,k}\phi_{i,j-1,k} + \widehat{\sigma}_{i,j,k-\frac12}\phi_{i,j,k-1} \\
&- \Big(\widehat{\sigma}_{i+\frac12,j,k} + \widehat{\sigma}_{i,j+\frac12,k} + \widehat{\sigma}_{i,j,k+\frac12} \\
&\quad + \widehat{\sigma}_{i-\frac12,j,k} + \widehat{\sigma}_{i,j-\frac12,k} + \widehat{\sigma}_{i,j,k-\frac12}\Big)\phi_{i,j,k}\Big). \qquad (2.3b)
\end{aligned}
$$

3. Fourier Analysis. In this section, we consider the system (1.6) and its discretization (2.1) under standard simplifying assumptions that allow us to conclude that the eigenvectors of all the blocks of A in (2.1) corresponding to scalar differential operators are Fourier modes. In particular, for discrete wavenumbers $0 \le \alpha, \beta, \gamma \le n-1$, we want the grid function $\psi^{\alpha\beta\gamma}$ given by

$$\psi^{\alpha\beta\gamma}_{ijk} := e^{(2\pi\alpha ih)\imath} e^{(2\pi\beta jh)\imath} e^{(2\pi\gamma kh)\imath} \qquad i,j,k = 0,1,\ldots n-1 \qquad (3.1)$$

to be an eigenvector of all the blocks of A in (2.1). This is true under the assumptions that

1. the boundary conditions are periodic;[2]
2. the grid is uniform; and
3. the material properties σ, ϵ, and μ are constant.

Under the first assumption, upon discretization, the indexing in (2.2) and (2.3) is done in arithmetic modulo n. For instance, grid points on, say, the top boundary are identified with opposite points on the bottom boundary, and centers of cells touching the top boundary are considered as neighbors of centers of cells opposite touching the bottom boundary. The scalar grid functions ${A^x}^h$, ${A^y}^h$, ${A^z}^h$, and ϕ^h each consist of $N := n^3$ unknowns, the matrix blocks in (2.1) are square of dimension $N \times N$, and the resulting system to be solved has dimension $4N \times 4N$.

Further, we make the quasi-static assumption (e.g., [29]) that $\widehat{\sigma} = \sigma$, and apply (1.8) to ensure $\sigma > 0$. This simplifies the presentation without loss of essence in the obtained theoretical results. In our experiments reported in Section 4, we drop this simplifying assumption in addition to all other assumptions of the present section.

Thus, the block matrix $\widehat{\sigma}^h$ reduces to σI, and the coefficient matrix in (2.1) can be written as

$$A = \begin{pmatrix} \Delta^h + \imath\omega\mu\sigma I_N & & & \imath\omega\mu\sigma D^h_x \\ & \Delta^h + \imath\omega\mu\sigma I_N & & \imath\omega\mu\sigma D^h_y \\ & & \Delta^h + \imath\omega\mu\sigma I_N & \imath\omega\mu\sigma D^h_z \\ -\sigma(D^h_x)^* & -\sigma(D^h_y)^* & -\sigma(D^h_z)^* & \sigma\Delta^h \end{pmatrix} \qquad (3.2)$$

[2]For a class of realistic geophysical problems, the fields are expected to vanish or decay in the absence of source currents, and the sources are frequently of compact support. Thus, for a sufficiently large domain Ω, the effect of boundary data on the fields inside the domain is often negligible. In such cases, the assumption of periodicity in the following analysis is particularly reasonable and does not compromise the model.

In (3.2), the matrices D_x^h, D_y^h, and D_z^h correspond to discretizations of first-order derivative operators with periodic boundary conditions. Assuming standard lexicographic ordering for the unknowns describing the grid functions,

$$\begin{aligned} D_x^h &:= I_n \otimes I_n \otimes D^- \in \mathbb{C}^{N\times N}, \\ D_y^h &:= I_n \otimes D^- \otimes I_n \in \mathbb{C}^{N\times N}, \text{ and} \\ D_z^h &:= D^- \otimes I_n \otimes I_n \in \mathbb{C}^{N\times N}. \end{aligned}$$

Here,

$$D^- := \frac{1}{h}\begin{pmatrix} 1 & & & -1 \\ -1 & 1 & & \\ & \ddots & \ddots & \\ & & -1 & 1 \end{pmatrix} \in C^{n\times n} \tag{3.3}$$

is the matrix for the periodic primitive backwards difference operator in one dimension, and $\otimes$ denotes the conventional Kronecker product (e.g., [13]). Likewise, the matrices $-(D_x^h)^*$, $-(D_y^h)^*$, and $-(D_z^h)^*$ in the fourth block row of (3.2) correspond to forward difference operators. Finally, the discretization Δ^h of the Laplacian operator Δ with periodic boundary conditions satisfies

$$\Delta^h = -D_x^h(D_x^h)^* - D_y^h(D_y^h)^* - D_z^h(D_z^h)^*.$$

The eigenvalues of these difference operators are

$$d_x{}^{\alpha\beta\gamma} := h^{-1}\left(1 - e^{-(2\alpha\pi h)\imath}\right) \text{ for } D_x^h, \tag{3.4a}$$

$$d_y{}^{\alpha\beta\gamma} := h^{-1}\left(1 - e^{-(2\beta\pi h)\imath}\right) \text{ for } D_y^h, \tag{3.4b}$$

$$d_z{}^{\alpha\beta\gamma} := h^{-1}\left(1 - e^{-(2\gamma\pi h)\imath}\right) \text{ for } D_z^h, \tag{3.4c}$$

$$\delta^{\alpha\beta\gamma} := -\frac{4}{h^2}\left(\sin^2(\alpha\pi h) + \sin^2(\beta\pi h) + \sin^2(\gamma\pi h)\right) \text{ for } \Delta^h, \tag{3.4d}$$

with common eigenvector $\psi^{\alpha\beta\gamma}$ as in (3.1). In particular, if $n > 2$ then $h < \frac{1}{2}$, and so the nonzero eigenvalues $\delta^{\alpha\beta\gamma}$ of Δ^h satisfy

$$0 < \frac{h^2}{12} \le -\frac{1}{\delta^{\alpha\beta\gamma}} \le \frac{h^2}{4\sin^2(\pi h)} < \frac{1}{16}, \quad \forall(\alpha,\beta,\gamma) \in K \tag{3.5a}$$

$$K := \{(\alpha,\beta,\gamma) : \alpha,\beta,\gamma = 0,\dots,n-1\} \backslash \{(0,0,0)\}. \tag{3.5b}$$

With the eigenvalues (3.4) of the blocks of A in (3.2), we want to determine the eigenvalues and singular values of the preconditioned iteration matrix $M^{-1}A$, where

$$M := \begin{pmatrix} \Delta^h & & & \\ & \Delta^h & & \\ & & \Delta^h & \\ & & & \sigma\Delta^h \end{pmatrix}. \tag{3.6}$$

The matrix M is real and consists of the dominant diagonal blocks of the matrix A (excluding the complex Helmholtz shift $\imath\omega\mu\sigma I_N$ in the first three block rows).

Note that the solution u of $\Delta u = b$ with periodic boundary conditions is determined only up to a constant. Thus, M in (3.6) has a zero eigenvalue of multiplicity four (corresponding to four distinct constant grid functions for A^{xh}, A^{yh}, A^{zh}, and ϕ^h). Likewise, A has a zero eigenvalue of multiplicity one. However, as in [11], if S_0 denotes the space spanned by the constant grid function $\psi^{000} \in \mathbb{C}^N$ and $S_0^\perp$ denotes the orthogonal complement of S_0 in $\mathbb{C}^N$, then $\Delta^h|_{S_0^\perp}$ is invertible. Further, the operator $(\Delta^h|_{S_0^\perp})^{-1}$ can be extended to an operator $(\Delta^h)_*^{-1}$ defined over all of $\mathbb{C}^N$ by defining it to be 0 on S_0. Thus, it makes sense to consider eigenvalue ranges for M and A which exclude the zero eigenvalues. This is achieved by imposing the condition

$$\alpha^2 + \beta^2 + \gamma^2 > 0,$$

as in (3.5b). Under this condition, with a slight abuse of notation, we subsequently refer to A and M as being nonsingular.

Having established that the blocks of A in (3.2) all share common eigenvectors and that considering the operator $M^{-1}A$ makes sense, we wish to derive bounds on the eigenvalue range and the l_2-condition number of $M^{-1}A$. The eigenvalues and singular values of this matrix can be determined by considering the eigenvalues of a 4×4 matrix with the same structure, as the following lemma indicates.

LEMMA 3.1. *Let $C \in \mathbb{C}^{(mn)\times(mn)}$ be a block matrix with blocks $C_{ij} \in \mathbb{C}^{n\times n}$ $(i, j = 1, \dots, m)$. Let the blocks C_{ij} all share a common eigenvector $\boldsymbol{v} \in \mathbb{C}^n$ with corresponding eigenvalues $\gamma_{ij} \in \mathbb{C}$ $(i, j = 1, \dots, m)$. Furthermore, let $G = (\gamma_{ij}) \in \mathbb{C}^{m\times m}$ have the eigenvalues γ_{ij} as its elements, and let λ be an eigenvalue of G with an eigenvector $\boldsymbol{u} \in \mathbb{C}^m$.*

Then λ is also an eigenvalue of C with an eigenvector $\boldsymbol{u} \otimes \boldsymbol{v}$.

Proof. Although this lemma is standard, we include the proof for completeness. By definition,

$$\begin{aligned} G\boldsymbol{u} &= \lambda \boldsymbol{u}, \text{ and} \\ C_{ij}\boldsymbol{v} &= \gamma_{ij}\boldsymbol{v} \qquad (i, j = 1, 2, \dots, m). \end{aligned}$$

Thus, the ith block of n values of $C(\boldsymbol{u} \otimes \boldsymbol{v})$ is

$$\begin{aligned} [C(\boldsymbol{u} \otimes \boldsymbol{v})]_i &= \sum_{j=1}^m C_{ij} u_j \boldsymbol{v} = \sum_{j=1}^m u_j \gamma_{ij} \boldsymbol{v} \\ &= \lambda u_i \boldsymbol{v} = \lambda \left[\boldsymbol{u} \otimes \boldsymbol{v}\right]_i . \end{aligned}$$

□

Next, we find the eigenvalues and singular values of the 4×4 matrix corresponding to $M^{-1}A$ in Fourier space. Recall the notation (1.9).

LEMMA 3.2. *Let $dx, dy, dz \in \mathbb{C}$ be prescribed scalars such that $\delta := -dx dx^* - dy dy^* - dz dz^* < 0$. Given $\sigma, \chi > 0$, define the complex 4×4 matrix $\widetilde{M}^{-1}\widetilde{A}$, where*

$$\widetilde{M} := \begin{pmatrix} \delta & & & \\ & \delta & & \\ & & \delta & \\ & & & \sigma\delta \end{pmatrix}, \ \textit{and} \qquad \widetilde{A} := \begin{pmatrix} \delta + \imath\chi & & & \imath\chi dx \\ & \delta + \imath\chi & & \imath\chi dy \\ & & \delta + \imath\chi & \imath\chi dz \\ -\sigma dx^* & -\sigma dy^* & -\sigma dz^* & \sigma\delta \end{pmatrix}.$$

Then, the eigenvalues $\widetilde{\lambda}$ *of* $\widetilde{M}^{-1}\widetilde{A}$ *are*

$$\widetilde{\lambda}_1 := 1 + \frac{\imath}{2\delta}\left(\chi + \sqrt{\chi(\chi - 4\delta\imath)}\right), \tag{3.7a}$$
$$\widetilde{\lambda}_2 = \widetilde{\lambda}_3 := 1 + \frac{\chi}{\delta}\imath, \tag{3.7b}$$
$$\widetilde{\lambda}_4 := 1 + \frac{\imath}{2\delta}\left(\chi - \sqrt{\chi(\chi - 4\delta\imath)}\right). \tag{3.7c}$$

Further, the singular values $\widetilde{\eta}$ *of* $\widetilde{M}^{-1}\widetilde{A}$ *are*

$$\widetilde{\eta}_1 := \left[1 + \frac{c}{2} + \frac{1}{2}\sqrt{c(c+4)}\right]^{\frac{1}{2}}, \tag{3.8a}$$
$$\widetilde{\eta}_2 = \widetilde{\eta}_3 := \left[1 + \frac{\chi^2}{\delta^2}\right]^{\frac{1}{2}}, \tag{3.8b}$$
$$\widetilde{\eta}_4 := \left[1 + \frac{c}{2} - \frac{1}{2}\sqrt{c(c+4)}\right]^{\frac{1}{2}}, \tag{3.8c}$$

where $c = c(-\frac{1}{\delta}, \chi) := \left(-\frac{1}{\delta}\right)\left(1 + \chi^2\left(1 - \frac{1}{\delta}\right)\right) > 0$.

Proof. Although the derivation of (3.7) and (3.8) requires substantial work, the verification of these formulae can be done by inspection. □

Note that the eigenvalues and singular values of $\widetilde{M}^{-1}\widetilde{A}$ in Lemma 3.2 depend only on the parameters $\delta < 0$ and $\chi > 0$. We next derive bounds for the eigenvalues (3.7) and the singular values (3.8) and hence bounds for their ranges.

LEMMA 3.3. *For all grids with widths* $h < 1/2$*, the eigenvalues* $\widetilde{\lambda}$ *of* $\widetilde{M}^{-1}\widetilde{A}$ *given in* (3.7) *satisfy*

$$0 < \widetilde{\lambda}_{min} \le \left|\widetilde{\lambda}\right| \le \widetilde{\lambda}_{max}$$

and the singular values $\widetilde{\eta}$ *given in* (3.8) *all satisfy*

$$0 < \widetilde{\eta}_{min} \le \widetilde{\eta} \le \widetilde{\eta}_{max},$$

where $\widetilde{\lambda}_{min}$, $\widetilde{\lambda}_{max}$, $\widetilde{\eta}_{min}$, *and* $\widetilde{\eta}_{max}$ *are positive constants that depend on* χ *but not on* δ. *Further,*

$$\frac{\widetilde{\lambda}_{max}}{\widetilde{\lambda}_{min}} = O(\chi^2) \text{ and } \frac{\widetilde{\eta}_{max}}{\widetilde{\eta}_{min}} = O(\chi^2).$$

Proof. For $h < 1/2$, we have $\delta < -16$ since $\delta^{\alpha\beta\gamma} < -16$ in (3.5a). Denote $\zeta = \sqrt{\chi^2 + 16\delta^2} > \chi$. From (3.7), we find

$$\left|\widetilde{\lambda}_1\right| = \left[\frac{\chi}{4\delta^2}\left(\chi + \zeta + \sqrt{2\chi}\sqrt{\zeta + \chi}\right) - \frac{\sqrt{2\chi}}{2\delta}\sqrt{\zeta - \chi} + 1\right]^{\frac{1}{2}},$$
$$\left|\widetilde{\lambda}_2\right| = \left|\widetilde{\lambda}_3\right| = \left[1 + \frac{\chi^2}{\delta^2}\right]^{\frac{1}{2}},$$
$$\left|\widetilde{\lambda}_4\right| = \left[\frac{\chi}{4\delta^2}\left(\chi + \zeta - \sqrt{2\chi}\sqrt{\zeta + \chi}\right) + \frac{\sqrt{2\chi}}{2\delta}\sqrt{\zeta - \chi} + 1\right]^{\frac{1}{2}}.$$

It follows that

$$|\widetilde{\lambda}_1| \geq |\widetilde{\lambda}_{2,3}| \geq |\widetilde{\lambda}_4|$$

for any valid choices of χ and δ. Examining $|\widetilde{\lambda}_1|$ and $|\widetilde{\lambda}_4|$ as δ varies over the interval $(-\infty, -16)$, we find

$$\widetilde{\lambda}_{\mathsf{max}} := \max\left\{\left|\widetilde{\lambda}_1\right| : \delta \in (-\infty, -16)\right\} = \frac{\chi}{16} + \frac{48}{\chi} + O\left(\frac{1}{\chi^3}\right).$$
$$\widetilde{\lambda}_{\mathsf{min}} := \min\left\{\left|\widetilde{\lambda}_4\right| : \delta \in (-\infty, -16)\right\} = \frac{16}{\chi} + O\left(\frac{1}{\chi^3}\right).$$

Thus,

$$\frac{\widetilde{\lambda}_{\mathsf{max}}}{\widetilde{\lambda}_{\mathsf{min}}} = \frac{\chi^2}{256} + O(1) = O(\chi^2).$$

Examining the singular values (3.8) in the same manner, we find

$$\widetilde{\eta}_1 \geq \widetilde{\eta}_{2,3} \geq \widetilde{\eta}_4.$$

Thus,

$$\widetilde{\eta}_{\mathsf{max}} := \max\left\{\widetilde{\eta}_1 : \delta \in (-\infty, -16)\right\} = \frac{\sqrt{17}}{16}\chi + O\left(\frac{1}{\chi}\right),$$
$$\widetilde{\eta}_{\mathsf{min}} := \min\left\{\widetilde{\eta}_4 : \delta \in (-\infty, -16)\right\} = \frac{16}{\sqrt{17}}\frac{1}{\chi} + O\left(\frac{1}{\chi^3}\right).$$

Hence,

$$\frac{\widetilde{\eta}_{\mathsf{max}}}{\widetilde{\eta}_{\mathsf{min}}} = \frac{17}{256}\chi^2 + O(1) = O(\chi^2).$$

□

The preceding lemmata give us the desired eigenvalues and singular values of the underlying matrix $M^{-1}A$ for the preconditioned system. Combining these results, we obtain:

THEOREM 3.4. *The eigenvalues of $M^{-1}A$ are given by*

$$\lambda_1^{\alpha\beta\gamma} = 1 + \frac{\imath}{2\delta^{\alpha\beta\gamma}}\left(\chi + \sqrt{\chi(\chi - 4\delta^{\alpha\beta\gamma}\imath)}\right), \tag{3.9a}$$

$$\lambda_2^{\alpha\beta\gamma} = \lambda_3^{\alpha\beta\gamma} := 1 + \frac{\chi}{\delta^{\alpha\beta\gamma}}\imath, \tag{3.9b}$$

$$\lambda_4^{\alpha\beta\gamma} = 1 + \frac{\imath}{2\delta^{\alpha\beta\gamma}}\left(\chi - \sqrt{\chi(\chi - 4\delta^{\alpha\beta\gamma}\imath)}\right), \tag{3.9c}$$

for $(\alpha, \beta, \gamma) \in K$. The singular values of $M^{-1}A$ are given by

$$\eta_1^{\alpha\beta\gamma} := \left[1 + \frac{c^{\alpha\beta\gamma}}{2} + \frac{1}{2}\sqrt{c^{\alpha\beta\gamma}(c^{\alpha\beta\gamma} + 4)}\right]^{\frac{1}{2}}, \tag{3.10a}$$

$$\eta_2^{\alpha\beta\gamma} = \eta_3^{\alpha\beta\gamma} := \left[1 + \frac{\chi^2}{{\delta^{\alpha\beta\gamma}}^2}\right]^{\frac{1}{2}}, \tag{3.10b}$$

$$\eta_4^{\alpha\beta\gamma} := \left[1 + \frac{c^{\alpha\beta\gamma}}{2} - \frac{1}{2}\sqrt{c^{\alpha\beta\gamma}(c^{\alpha\beta\gamma} + 4)}\right]^{\frac{1}{2}}, \tag{3.10c}$$

where $c^{\alpha\beta\gamma} = c(-\frac{1}{\delta^{\alpha\beta\gamma}}, \chi) := \left(-\frac{1}{\delta^{\alpha\beta\gamma}}\right)\left(1 + \chi^2\left(1 - \frac{1}{\delta^{\alpha\beta\gamma}}\right)\right) > 0$ *and* $(\alpha, \beta, \gamma) \in K$.

Furthermore, the eigenvalues and singular values of $M^{-1}A$ *are bounded above and below independent of the grid size* h*, provided* $h < 1/2$*. Defining*

$$\lambda_{min} = \min\{|\lambda_i| : 1 \le i \le 4\}, \qquad \lambda_{max} = \max\{|\lambda_i| : 1 \le i \le 4\},$$
$$\eta_{min} = \min\{\eta_i : 1 \le i \le 4\}, \qquad \eta_{max} = \max\{\eta_i : 1 \le i \le 4\},$$

the eigenvalue range $\lambda_{max}/\lambda_{min}$ *and the condition number* η_{max}/η_{min} *are bounded independent of the grid, but increase quadratically with the parameter* $\chi = \omega\mu\sigma$*:*

$$\frac{\lambda_{max}}{\lambda_{min}} \le \frac{\widetilde{\lambda}_{max}}{\widetilde{\lambda}_{min}} = O(\chi^2) \text{ and } \frac{\eta_{max}}{\eta_{min}} \le \frac{\widetilde{\eta}_{max}}{\widetilde{\eta}_{min}} = O(\chi^2).$$

Proof. The eigenvalues (3.9) and singular values (3.10) of $M^{-1}A$ are derived directly from the eigenvalues (3.7) and singular values (3.8) of $\widetilde{M}^{-1}\widetilde{A}$ in Lemma 3.2 by applying Lemma 3.1. Then, the bounds $\widetilde{\lambda}_{\mathsf{max}}/\widetilde{\lambda}_{\mathsf{min}}$ and $\widetilde{\eta}_{\mathsf{max}}/\widetilde{\eta}_{\mathsf{min}}$ follow from Lemma 3. ☐

In Figure 3.1, we plot the curves based on the above estimates for the eigenvalue range and the condition number of $\widetilde{M}^{-1}\widetilde{A}$ as a function of χ (which are in fact the bounds $\widetilde{\lambda}_{\mathsf{max}}/\widetilde{\lambda}_{\mathsf{min}}$ and $\widetilde{\eta}_{\mathsf{max}}/\widetilde{\eta}_{\mathsf{min}}$ from Lemma 3.3). We also plot the actual values of $\lambda_{\mathsf{max}}/\lambda_{\mathsf{min}}$ and $\eta_{\mathsf{max}}/\eta_{\mathsf{min}}$ as computed from Theorem 3.4 in the case $n = 10^4$.

Notice that Lemma 3.3 also indicates that the ratio of the largest to smallest eigenvalues significantly underestimates the ratio of the largest to smallest singular values (which is the l_2-condition number) in the case that χ is large. This is also reflected in a lower degree of diagonal dominance in A and $M^{-1}A$ (for a fixed mesh size h) as ω increases.

The practical implication of Theorem 3.4 is that the number of iterations required for convergence (up to a set positive tolerance) of a Krylov method for (3.2) preconditioned by the real parts of the leading blocks is expected to be small and independent of the grid size. As the frequency ω increases in a range where $\omega\mu\sigma \gg 1$, the number of iterations may be expected to increase like ω^2.

The full inversions of the Laplacians on the main block diagonal of M may seem excessive for preconditioning purposes. Instead, we now consider applying just one multigrid cycle. Denote by B the approximate inverse for M obtained in this way. It is well-known (e.g., [17, 30]) that for a W-cycle using standard grid transfer and coarse grid operators and a sufficiently good smoothing rate (which may be achieved, e.g., by two (point) red-black Gauss-Seidel sweeps before and after the coarse grid correction), there is a constant c such that, independent of the grid size,

$$\|I - BM\| \le c < 1.$$

This implies, in particular, that the condition number of BM is bounded. But writing

$$\mathrm{cond}(BA) \le \mathrm{cond}(BM)\ \mathrm{cond}(M^{-1}A)$$

and applying Theorem 3.4 now yields similar results for the one-multigrid-cycle preconditioner:

COROLLARY 3.5. *The condition number of* BA*, where* B *is the preconditioning effect of one multigrid W-cycle, is bounded independent of the grid size* h*. This condition number increases quadratically with the parameter* $\chi := \omega\mu\sigma$*.*

FIG. 3.1. *Eigenvalue range $\widetilde{\lambda}_{max}/\widetilde{\lambda}_{min}$ and the condition number $\widetilde{\eta}_{max}/\widetilde{\eta}_{min}$ as a function of χ, based on the formulae in Lemma 3.3; also plotted are actual values ($\lambda_{max}/\lambda_{min}$ and η_{max}/η_{min}, respectively) for $n = 10^4$.*

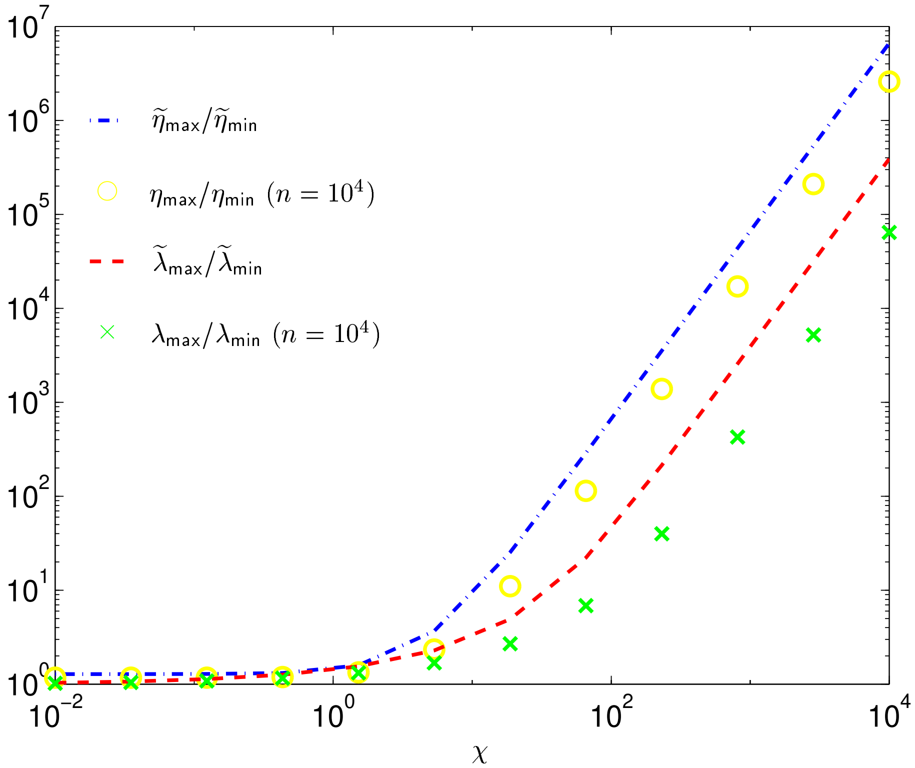

4. Numerical Experiments. In the following experiments, the parameters $\epsilon = \epsilon_0 = 8.8542 \times 10^{-12}$ F/m and the permittivity $\mu = \mu_0 = 4\pi \times 10^{-7}$ H/m are fixed constants. The domain Ω is the cube $[-1,1]^3$ and the homogeneous boundary conditions (1.7) are imposed on $\partial\Omega$ as described in Section 2. As in [2, 15, 16], the grids used are either uniform or exponentially-widening, and preconditioned BiCGStab [3] is used to solve the linear systems generated by the discretization. As a convergence criterion for all BiCGStab iterations, we require a reduction of the relative residual to within a tolerance of 10^{-7}. Results from all experiments are given in terms of iteration counts.

We contrast the performances of several preconditioning strategies.

1. Exact solves of diagonal blocks (M_E): The real parts of the diagonal blocks, namely
$$\operatorname{diag}\left(\Delta^h + \omega^2\epsilon I, \Delta^h + \omega^2\epsilon I, \Delta^h + \omega^2\epsilon I, (\nabla\cdot)^h\sigma^h(\nabla)^h\right),$$
are inverted exactly (by iterating a multigrid solver to convergence) in each iteration. For the magnitudes of $\omega^2\epsilon$ considered, the difference between this preconditioning strategy and the one analyzed in Section 3 is negligible.
2. Multigrid preconditioning (M_M): Single V(2,1)-cycles [7, 17] are applied for each of the diagonal blocks to approximate the effect of M_E. For the (1,1), (2,2), and (3,3) blocks, we use point red-black Gauss-Seidel smoothing if the

grid is uniform, and alternating-plane smoothing otherwise. For the (4,4) block, we use alternating-plane smoothing regardless of the grid.

3. ILU preconditioning (M_I): An incomplete-LU factorization is computed (see [25, 3]) using the real part of the whole coefficient matrix A (ie. not just the diagonal blocks). We use 10^{-2} for the drop tolerance.
4. SSOR preconditioning (M_S): We use the value 1.0 for the over-relaxation parameter [3].

The multigrid solver used is Dendy's code BOXMG (a blackbox multigrid solver, see [9, 10]). For Poisson or simple Helmholtz problems on uniform grids, point red-black Gauss-Seidel smoothing cheaply inverts the $(1,1)$, $(2,2)$, and $(3,3)$ blocks. For the anisotropic diffusion operator in the (4,4) block and problems on non-uniform grids alternating-plane smoothing is required to achieve reasonable multigrid performance, as observed in [1, 9, 10]; hence, the more expensive plane relaxations are employed. This gives a slight cause for concern, since the implementation of alternating-plane smoothing is quite costly; however, for large highly anisotropic problems, the multigrid preconditioner applied with alternating-plane smoothing yields a robust solver.

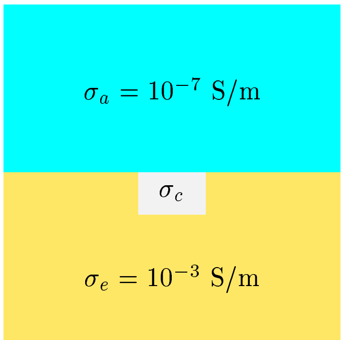

FIG. 4.1. *Cross-section of a conducting block in a half-space*

For the conductivity σ in Ω, we choose

$$\sigma(x,y,z) = \begin{cases} \sigma_a, & z > 0; \\ \sigma_c, & |x| \le \frac{1}{5}, |y| \le \frac{1}{5}, -\frac{1}{5} \le z \le 0; \\ \sigma_e, & \text{otherwise}, \end{cases}$$

for the experiments. This models a conducting block of conductivity σ_c embedded in a half-space (ie. at the interface between ground and air). The conductivity σ_e of the earth is $\sigma_e = 10^{-3}$ S/m and the conductivity σ_a of the air is $\sigma_a = 10^{-7}$ S/m (which regularizes σ as in (1.8)).

Thus, in our experiments, we vary the parameters σ_c and ω to compare performances of various preconditioners. We also vary the source term $\boldsymbol{J^s}$ in (1.6); the applied electromagnetic sources are electric dipoles or magnetic current loops as in [15, 29].

Consider first varying ω over the moderate range $[10^0, 10^4]$ Hz, and varying σ_c over the range $[10^{-2}, 10^2]$ S/m. These ranges translate to the parameter χ in (1.9) lying in the interval $[4\pi \times 10^{-9}, 4\pi \times 10^{-1}]$. The jump discontinuities in σ for this range of σ_c are between 5 and 9 orders of magnitude. For an electric dipole source, the results when discretized on uniform and nonuniform grids are tabulated in Tables 4.1 and 4.2 respectively. Tables 4.3 and 4.4 present results from similar trials on uniform and nonuniform grids respectively with a magnetic (divergence-free) source term instead.

Uniform grids													
σ_c (S/m)	# of cells	$\omega = 10^0$Hz				$\omega = 10^2$Hz				$\omega = 10^4$Hz			
		M_E	M_M	M_I	M_S	M_E	M_M	M_I	M_S	M_E	M_M	M_I	M_S
10^{-2}	10^3	1	3	7	19	3	3	7	19	6	6	11	20
	20^3	2	2	13	34	2	2	13	34	5	5	22	35
	30^3	2	2	20	44	3	3	20	44	5	5	34	50
	40^3	3	3	27	58	3	3	27	61	5	5	46	70
	50^3	3	3	33	72	3	3	33	79	5	5	61	86
10^0	10^3	3	3	9	25	3	3	9	25	6	6	12	25
	20^3	3	3	18	44	3	3	19	44	5	5	35	48
	30^3	3	3	30	66	3	3	30	50	5	5	56	63
	40^3	3	3	41	73	3	3	41	73	5	5	66	82
	50^3	3	3	44	100	3	3	44	100	5	5	100	111
10^2	10^3	3	3	9	20	3	3	9	25	6	6	12	25
	20^3	3	3	20	44	3	3	20	44	6	6	37	48
	30^3	3	3	30	67	3	3	27	59	6	6	55	67
	40^3	3	3	40	73	3	3	40	73	6	6	76	86
	50^3	3	3	49	95	3	3	48	96	6	6	97	109

TABLE 4.1
BiCGStab iterations with an electric dipole source and uniform grids.

Nonuniform grids													
σ_c (S/m)	# of cells	$\omega = 10^0$Hz				$\omega = 10^2$Hz				$\omega = 10^4$Hz			
		M_E	M_M	M_I	M_S	M_E	M_M	M_I	M_S	M_E	M_M	M_I	M_S
10^{-2}	30^3	1	3	18	47	3	3	18	49	5	5	34	52
	40^3	4	4	27	59	4	4	26	64	7	7	40	68
	50^3	2	2	28	76	2	2	28	71	4	4	48	84
10^0	30^3	3	3	26	65	3	3	26	62	5	5	55	76
	40^3	4	4	31	76	4	4	34	78	7	7	76	91
	50^3	2	2	43	101	2	2	43	102	4	4	98	139
10^2	30^3	3	3	25	65	3	3	25	64	6	6	53	76
	40^3	4	4	31	79	4	4	34	80	7	7	76	102
	50^3	2	2	43	105	2	2	43	102	5	5	100	132

TABLE 4.2
BiCGStab iterations with an electric dipole source and nonuniform grids.

All of the trials summarized in Tables 4.1–4.4 clearly show evidence of grid-independent rates of convergence of the Krylov method when preconditioned by M_E or M_M, as opposed to M_I or M_S. In spite of the seemingly strong restrictions of the Fourier analysis of Section 3, the convergence behavior of the exact block inversion M_E measures up to theoretical predictions. That is, the analysis succeeds in capturing the essential local behavior of discrete operators for physically reasonable problems unhindered by the additional complications of nonuniform grids, of different boundary conditions, and, most significantly, of highly discontinuous conductivity models.

The results also show virtually identical performance in terms of iteration counts for the exact preconditioner M_E versus the single multigrid V(2,1)-cycle M_M. This observation suggests that solving the diagonal blocks exactly is unnecessary, at least within this frequency range. In particular, single V(2,1)-cycles work as effectively as the preconditioner M_E, with considerable savings in computational work.

Another interesting aspect of these results is that the iteration counts for all the

Uniform grids													
σ_c	# of	$\omega = 10^0$Hz				$\omega = 10^2$Hz				$\omega = 10^4$Hz			
(S/m)	cells	M_E	M_M	M_I	M_S	M_E	M_M	M_I	M_S	M_E	M_M	M_I	M_S
10^{-2}	10^3	1	4	6	13	4	4	6	13	4	4	6	13
	20^3	4	4	13	25	4	4	13	25	4	4	15	25
	30^3	4	4	19	32	4	4	19	32	4	4	21	32
	40^3	4	4	27	42	4	4	27	42	4	4	32	41
	50^3	4	4	32	51	4	4	32	53	4	4	36	53
10^0	10^3	4	4	6	13	4	4	6	13	4	4	6	13
	20^3	4	4	13	25	4	4	13	25	4	4	15	25
	30^3	4	4	19	32	4	4	19	32	4	4	21	32
	40^3	4	4	27	43	4	4	27	41	4	4	32	43
	50^3	4	4	32	51	4	4	32	51	4	4	37	48
10^2	10^3	5	5	7	13	5	5	7	13	5	5	7	13
	20^3	5	5	13	26	5	5	13	26	5	5	15	26
	30^3	4	4	19	32	4	4	19	32	4	4	22	32
	40^3	5	5	27	42	5	5	27	42	5	5	32	43
	50^3	5	5	31	52	5	5	31	50	5	5	37	56

TABLE 4.3
BiCGStab iterations with a magnetic source and uniform grids.

Nonuniform grids													
σ_c	# of	$\omega = 10^0$Hz				$\omega = 10^2$Hz				$\omega = 10^4$Hz			
(S/m)	cells	M_E	M_M	M_I	M_S	M_E	M_M	M_I	M_S	M_E	M_M	M_I	M_S
10^{-2}	30^3	1	3	23	41	3	3	23	42	3	3	25	42
	40^3	3	3	30	45	3	3	30	50	3	3	36	51
	50^3	2	2	37	61	2	2	37	60	2	2	47	62
10^0	30^3	3	3	23	42	3	3	23	41	3	3	26	41
	40^3	3	3	30	47	3	3	30	44	3	3	37	48
	50^3	3	3	37	60	3	3	37	65	3	3	47	65
10^2	30^3	3	3	21	41	3	3	21	41	4	4	27	48
	40^3	4	4	30	54	4	4	30	49	4	4	37	49
	50^3	3	3	37	57	3	3	37	57	4	4	47	59

TABLE 4.4
BiCGStab iterations with a magnetic source and nonuniform grids.

preconditioners do not appear to depend strongly on ω or σ_c. Looking at Figure 3.1, we see that the spread of eigenvalues and the l_2-condition number is quite flat until $\chi \simeq 10^1$. Once χ gets larger, however, the quadratic dependence of both quantities on χ becomes apparent and we can see the condition number getting far worse. Since χ is at most $4\pi \times 10^{-1}$ in the trials so far, we do not observe the iterations changing much as σ_c and ω are varied within this range.

	# of	ω (Hz)					
	cells	10^1	10^2	10^3	10^4	10^5	10^6
M_M	30^3	3	3	3	6	12	98
	40^3	3	3	3	6	13	116
	50^3	3	3	3	6	12	128
M_I	30^3	30	27	31	55	166	642
	40^3	40	40	42	76	210	1180
	50^3	46	48	51	97	273	1551

TABLE 4.5
BiCGStab iterations for $\sigma_c = 10^2$ S/m for a range of frequencies.

To better observe the effect of increasing the parameter χ, we fix the underlying conductivity model with $\sigma_c = 10^2$ S/m and vary the frequency ω over a larger range. For these trials, we use an electric dipole source and count the number of iterations to convergence with problems discretized on uniform grids. We restrict our attention to the multigrid preconditioner M_M and the ILU preconditioner M_I. The results are summarized in Table 4.5.

Table 4.5 demonstrates the degradation of the both preconditioning strategies M_M and M_I with increasing frequency. As in the other trials, iteration counts for the ILU-preconditioned system grow as the grid is refined, as opposed to the grid-independent number of iteration counts observed for the multigrid-preconditioned system. At the highest frequency $\omega = 10^6$ Hz, $\chi \approx 4\pi$. Indeed, the performance of the preconditioners worsens in increasing ω from 10^5 Hz to 10^6 Hz . This is consistent with the sharp rise we observe in $\widetilde{\eta}_{\mathsf{max}}/\widetilde{\eta}_{\mathsf{min}}$ in Figure 3.1 near $\chi \simeq 10^1$. Thus, the observations in a physically realistic example agree well with the predictions of our Fourier analysis.

The CPU-time required for each iteration[3] of the multigrid preconditioner was found to be roughly 4 times more than that for the ILU preconditioner in case of a uniform grid, and roughly 8.5 times more in the case of the exponentially widening grid (due to the additional cost of alternating-plane relaxations). Thus, using the ILU preconditioner M_I actually resulted in a faster algorithm than using the multigrid preconditioner M_M, for coarse discretizations. But for fine discretizations (e.g., all cases recorded in Table 4.5) the multigrid preconditioner was found to be significantly more efficient. Obviously, there is a crossover point beyond which the multigrid preconditioner is more efficient, since it achieves convergence to a fixed tolerance within a constant number of iterations independent of the grid spacing h. In this example we see, moreover, that the crossover point occurs for grid sizes which are well within practical range. We feel that a more specific implementation of the multigrid cycle could improve the the efficiency of the preconditioner further, and lead to an earlier crossover point.

The results presented here have been based on a single geophysical model. We have also performed tests with other models presented in [15, 16] with qualitatively similar results.

Perhaps the greatest beauty of our multigrid approach as such is that indeed the part which is hard to program is within a black box code, already written by someone else. This is to be contrasted with all-out multigrid efforts such as [18], which achieve rapid convergence results but at a price in transparency and modularity (see also [4, 14]). A complete multigrid approach may perform better in cases where μ has large jump discontinuities, however, and we plan to address this in the future.

Acknowledgments. We thank Drs. J.D. Moulton and J. Dendy for very generous assistance in using BOXMG. We also thank Drs. E. Haber and D. Oldenburg for many helpful discussions.

REFERENCES

[1] R. E. Alcouffe, A. Brandt, J. E. Dendy, and J. W. Painter, *The multi–grid methods for the diffusion equation with strongly discontinuous coefficients*, SIAM J. Sci. Stat. Comput., 2 (1981), pp. 430–454.

[3]The iteration times were compared by running trials with the preconditioners M_M and M_I on various machines. Precise computational work estimates for BOXMG can be found in [10, 9].

[2] D. Aruliah, U. Ascher, E. Haber, and D. Oldenburg, *A method for the forward modelling of 3D electromagnetic quasi-static problems*, M3AS, (1999). To appear.
[3] R. Barrett, M. Berry, T. Chan, J. Demmeland, J. Donato, J. Dongarra, V. Eijkhout, R. Pozo, C. Romine, and H. V. der Vorst, *Templates for the Solution of Linear Systems: Building Blocks for Iterative Methods*, SIAM, Philadelphia, 1994.
[4] R. Beck, *Algebraic multigrid by component splitting for edge elements on simplicial triangulations*, tech. report, Konrad-Zuse-Zentrum, 1999.
[5] R. Beck, P. Deuflhard, R. Hiptmair, R. Hoppe, and B. Wohlmuth, *Adaptive multilevel methods for edge element discretizations of maxwell's equations*, Surveys Math. Indust., 8 (1999), pp. 271–312.
[6] A. Bossavit, *Computational electromagnetism. Variational formulation, complementarity, edge elements*, Academic Press, 1998.
[7] A. Brandt, *Multigrid techniques: 1984 Guide with applications to fluid Dynamics*, The Weizmann Institute of Science, Rehovot, Israel, 1984.
[8] T. Chan and H. Elman, *Fourier analysis of iterative methods for elliptic boundary value problems*, SIAM Review, 31 (1989), pp. 20–49.
[9] J. Dendy, Jr., *Two multigrid methods for three-dimensional problems with discontinuous and anisotropic coefficients*, SIAM J. Sci. Stat. Comp., 8 (1987), pp. 673–685.
[10] J. E. Dendy, *Black box multigrid*, Journal of Computational Physics, 48 (1982), pp. 366–386.
[11] H. Elman, *Preconditioning for the steady-state Navier-Stokes equations with low viscosity*, SIAM J. Scient. Comput., 20 (1999), pp. 1299–1316.
[12] M. Everett and A. Schultz, *Geomagnetic induction in a heterogenous sphere: Azimuthally symmetric test computations and the response of an undulating 660-km discontinuity*, J. Geophys. Res., 101 (1996), pp. 2765–2783.
[13] G. Golub and C. V. Loan, *Matrix Computations*, Johns Hopkins University Press, 1983.
[14] J. Gopalakrishnan and J. Pasciak, *Overlapping Schwarz preconditioners for indefinite Maxwell equations*. Manuscript.
[15] E. Haber and U. Ascher, *Fast finite volume simulation of 3D electromagnetic problems with highly discontinuous coefficients*, SIAM J. Scient. Comput., (2001). To appear.
[16] E. Haber, U. Ascher, D. Aruliah, and D. Oldenburg, *Fast simulation of 3D electromagnetic using potentials*, J. Comput. Phys., 163 (2000), pp. 150–171.
[17] W. Hackbusch, *Multi-Grid methods and Applications*, Springer-Verlag, 1985.
[18] R. Hiptmair, *Multigrid method for Maxwell's equations*, SIAM J. Numer. Anal, 36 (1998), pp. 204–225.
[19] J. Jin, *The Finite Element Method in Electromagnetics*, John Wiley and Sons, 1993.
[20] J. D. Moulton, *Numerical implementation of nodal methods*, PhD thesis, Institute of Applied Mathematics, University of British Columbia, 1996.
[21] G. Newman, *Three dimensional magnetotelluric modeling and inversion*, Proceedings of the Second Symposium on 3D Electromagnetics, (1999). Salt Lake City Utah.
[22] G. Newman and D. Alumbaugh, *Frequency-domain modelling of airborne electromagnetic responses using staggered finite differences*, Geophys. Prospecting, 43 (1995), pp. 1021–1042.
[23] I. Perugia, V. Simoncini, and M. Arioli, *Linear algebra methods in a mixed approximation of magnetostatic problems*, SIAM J. Scient. Comput., 21 (1999), pp. 1085–1101.
[24] R. Richtmyer and K. Morton, *Difference Methods for Initial-Value Problems*, Wiley, 1967.
[25] Y. Saad, *Iterartive Methods for Sparse Linear Systems*, PWS Publishing Company, 1996.
[26] S. Selberherr, *Analysis and Simulation of Semiconductor Devices*, Wien: Springer-Verlag, 1984.
[27] T. J. Smith, *Conservative modeling of 3D electromagnetic fields; part I: properties and error analysis*, Geophysics, 61 (1996), pp. 1308–1318.
[28] A. Taflove, *Computational Electrodynamics: the Finite-Difference Time-Domain Method*, Artech House Publishers, 1995.
[29] C. Weaver, *Mathematical Methods for Geo-Electromagnetic Induction*, John Wiley & Sons Inc, Philadelphia, 1994.
[30] P. Wesseling, *An Introduction to Multigrid Methods*, John Wiley & Sons, Chichester, 1992.